Interaction Between Precipitate Basal Plates and Tensile Twins in Magnesium Alloys

P. HIDALGO-MANRIQUE and J.D. ROBSON

A textured Mg-Al-Zn alloy rolled plate was solution-treated and then aged at 320 °C for 2 and 116 hours, respectively. Afterwards, the three conditions were tested at room temperature in compression along the transverse direction to activate $\{10\bar{1}2\}$ twinning. Both aged specimens exhibited a yield stress about 10 MPa higher than that of the solution-treated condition, with the increase of the yield stress attributed to the extra stress required for the twins to grow in the presence of particles. In order to understand the mechanism responsible for such strengthening, the effect of the precipitate basal plates on the critical resolved shear stress (CRSS) for twin growth was estimated using four different calculation approaches: Orowan stress to bow twinning dislocations around particles, elastic back-stress resulting from unsheared precipitates inside the twin, strengthening of basal slip within the twin (related to plastic relaxation), and stress to bow a twinning super-dislocation loop capable of further expansion. These methods give an order of magnitude difference in the calculated strengthening effect that spans the measured CRSS increase. The last two methods give the best estimates of the CRSS increase for twin growth depending on the aging time.

https://doi.org/10.1007/s11661-019-05301-1

I. INTRODUCTION

WROUGHT Mg parts usually exhibit a remarkable yield stress asymmetry at room temperature (RT), with a factor 2 difference in strength not uncommon when tested in compression and tension along the same axis.[1–4] This asymmetry hinders the wider utilization of Mg in structural applications and means that the potential of Mg to greatly reduce weight and increase fuel efficiency in transport applications is not fully exploited.

Mechanical asymmetry is mainly associated with the strong crystallographic texture developing in Mg during the most common processing techniques[5,6] and the polar nature of twinning, since the easy twinning mode is active only when there is an extension component parallel to the *c*-axis.[7] Therefore, at RT, in textured rolled sheets, where the basal planes preferentially orientate parallel to the rolling plane, when testing along the in-plane directions, extension twinning is active under compression, whereas prismatic slip is active under tension.[8] The critical resolved shear stress (CRSS) for both deformation systems is different,[9,10] which results in the above-mentioned yield stress asymmetry, with the yield stress being higher in tension than in compression. The same phenomenon is also observed in extrusions when loading along the extrusion direction, and has the same fundamental origin.[11,12]

One approach to overcoming this problem is to modify (weaken) the texture by adding certain elements,[13–17] changing the conditions of classical thermomechanical processing techniques[18–20] or using more complex strain paths like equal channel angular extrusion (ECAE).[21,22] However, these approaches also add considerably to the cost of the product, either through the introduction of expensive elements (*e.g.*, rare earths) or more complex process pathways (*e.g.*, ECAE). Moreover, texture weakening can only lead to a reduction in asymmetry by reducing overall strength as it works by enabling yield to be controlled in all orientations by low CRSS modes (*e.g.*, basal slip).

Another way to attenuate the RT yield stress asymmetry of textured Mg consists in decreasing the $CRSS_{prismatic}/CRS_{twinning}$ ratio, so that the activity of prismatic slip is enhanced at the expense of twinning. Since the sensitivity to grain size is higher for twinning than for slip,[23,24] grain refinement is one possibility. However, optimizing the processing conditions in order to attain fine enough grain sizes may be very time-consuming and not practical. Solute additions and precipitation are other possibilities as it is known that solutes[25,26] and precipitates[27–43] do not strengthen all

P. HIDALGO-MANRIQUE, and J.D. ROBSON are with the School of Materials, University of Manchester, MSS Tower, Manchester M13 9PL, UK. Contact e-mail: paloma.hidalgo-manrique@manchester.ac.uk

Manuscript submitted July 18, 2018.
Article published online May 29, 2019

the deformation mechanisms equally and indeed, solute atoms may even soften prismatic slip.[25,44] However, it is unlikely that the differential strengthening effect provided by solute is as large as to eliminate asymmetry. On the contrary, optimal distributions of precipitates can produce this effect. For this reason, precipitation is considered to be an important tool for controlling the balance between prismatic slip and twinning, which is, in turn, affected by the precipitate shape and habit.[27,31,36] In this way, while precipitation of basal plates reduces asymmetry in strongly textured Mg-Al-Zn alloys[29,33,35] through the preferential strengthening of twinning, precipitation of *c*-axis rods in Mg-Zn alloys causes the opposite effect.[28,40]

Since this approach is based on inhibiting twinning by precipitation, understanding how precipitates influence twinning is paramount to control the RT mechanical asymmetry of Mg wrought products. Twinning consists of nucleation and growth and both processes may be affected by the presence of precipitates. It has been experimentally demonstrated that particles do not suppress twin nucleation in Mg alloys. In fact, while the twin volume fraction decreases[28–30] or remains invariant,[35,40,41] precipitation leads in some alloys to a higher number of narrower twins, even for lamellar precipitate structures.[35] These observations suggest that particles suppress twin growth more strongly than they suppress twin nucleation.

Depending on the relative size of the growing twin and the precipitate, twins and particles interact in different ways in Mg. Large particles can stop twins, although twinning can continue by the nucleation of new twins in the matrix on the far side of the particles.[35,36] Small particles are engulfed by twins, where they can remain unsheared[28,31,33,36,40,45,46] or being sheared.[32,47] Precipitates are sheared by twins only when they are very fine or coherent. More commonly, particles are not sheared, although they can undergo a rigid body rotation inside the twin in order to accommodate part of the twinning shear.[31–33,36] Another common observation is that twin boundaries become deflected when they intersect particles, indicating that particles provide a resistance to the migration of twin boundaries.[29,36] Gharghouri *et al.*[46] even showed that twins avoid intersection with a particle by changing their apparent habit plane, further confirming that precipitates hinder twin propagation.

Despite all these experimental evidences that particles can have a strong effect on twinning in Mg, the mechanisms by which particles interact with twinning dislocations are less clear than the interaction mechanisms of particles with slip dislocations. So, in the case of slip, there is fairly good agreement between the precipitate strengthening predicted by the Orowan expression and the experimental results.[27,28,30,31,33,34,36,43] On the contrary, the Orowan model, based on the bowing of dislocations around shear-resistant particles, does not fully account for the hardening of the twin system produced by precipitates.[28,30,31,33,36,40,43] Therefore, there must be additional contributions from other mechanisms like the back-stress arising from the elastic deformation of particles, the hardening of the slip systems that accommodate twinning or the stress required to bow a super-dislocation around particles.[28,31,33,36,40,41,43,48] However, more systematic studies of the influence of particle morphology, orientation, volume fraction, size, and spacing on twinning are still needed before we can fully describe how precipitates affect twinning and thus predict the strengthening caused by particles in Mg.

The purpose of this study was to investigate the interaction between twins and large-sized basal plates in a system containing a large volume fraction of precipitates. For this purpose, an AZ80 Mg alloy rolled plate, exhibiting basal texture, was compressed at RT along the transverse direction (TD) in the solution-treated and two different aged conditions. High resolution scanning electron microscopy was used to analyze the distribution of precipitates in the aged samples and to examine the effect of precipitate characteristics on twinning. This has enabled a greater number of twin/particle interactions to be studied over a larger area than by using transmission electron microscopy. From measurements of particles parameters, the strengthening increment has been calculated using four different methods in the literature. These calculations have been compared with the measured strengthening increment and used to identify the likely dominant factors that determine the strengthening effect.

II. EXPERIMENTAL PROCEDURE

The starting material in this work was a cast AZ80 (Mg-7.5 wt pct Al-0.5 wt pct Zn) alloy. From the cast ingot, a billet (9.6 cm long, 5 cm wide and 3 cm thick) was cut out. This billet was homogenized at 400 °C for 24 hours followed by air-cooling. The homogenized billet was rolled at 400 °C in lubricated conditions to a true strain of around 1, in five passes, followed by water-cooling. The inter-pass annealing time was approximately 5 minutes. The rolled plate was solution-treated at 420 °C for 1 hour. Afterwards, two portions of the plate were aged at 320 °C for 2 hours (aging treatment 1) and 116 hours (aging treatment 2), respectively. This aging temperature was chosen because it led to the formation of uniform distributions of large continuous $Mg_{17}Al_{12}$ precipitate basal plates. With the idea of preserving the microstructure, the specimens were immediately water-quenched upon the completion of the solution and the aging heat treatments. Vickers microhardness tests with a load of 0.5 kg were used to monitor the age-hardening response. It was observed that the hardness reached a value of ~ 70 VHN after 1 to 2 hours of aging, but remained essentially constant at this value with increasing the aging time up to ~ 116 hours. This means that, although the two selected aged conditions exhibit the same hardness, the aged 1 condition (aged for 2 hours) corresponds to the peak-aged state, while the aged 2 condition (aged for 116 hours) is an over-aged sample.

Compression cylinders with a diameter of 7 mm and a height of 10.5 mm were machined from the solution-treated and aged portions of the rolled plate, their

loading axis being parallel to the TD. They were uniaxially compressed at RT on a universal Instron machine using a constant rate of crosshead displacement corresponding to an initial strain rate of 10^{-3} s^{-1}. The compression tests were performed in lubricated conditions both to failure and to intermediate strains. After correcting for the machine compliance, the true stress (σ) and true strain (ε) curves were calculated using the load-displacement data from the load frame. The yield stress was estimated as the true stress at an engineering strain of 0.2 pct and the work hardening rate was estimated as $d\sigma/d\varepsilon$.

Microstructural characterization was performed by optical microscopy (OM) and by scanning electron microscopy (SEM) in a Zeiss EVO60 equipment and in a Sirion field emission gun microscope. The latter, equipped with a HKL system, was also used to carry out electron back-scattered diffraction (EBSD) measurements. The macrotexture was analyzed by X-ray diffraction (XRD). The experimental pole figures were measured using Cu K_α radiation in a Bruker D8 Discover diffractometer. From these data, the orientation distribution function and the calculated pole figures were obtained using the MATLAB toolbox MTEX. The inverse pole figures were then derived from the calculated direct pole figures. Sample preparation consisted of manual grinding and polishing down to 1 μm with SiC papers and diamond suspensions. In addition, for OM and SEM, the samples were chemically etched in acetic picral and nital solutions, while for EBSD, they were final polished in colloidal silica.

III. RESULTS

A. *Characterization of Initial Microstructures*

Figure 1 illustrates OM micrographs of the solution-treated and aged materials. The insets in these micrographs show the average grain sizes, which have been determined by the linear intercept method from five different micrographs. Five randomly positioned line segments were drawn on the micrographs, so that about 440 measurements were made for each condition. It can be seen that the three samples exhibit a fully recrystallized microstructure with a uniform grain size distribution. It is interesting to note that the grain size only increases from 31 ± 5 μm after the solution treatment to 37 ± 6 μm after aging for 116 hours, which means that the effect of aging at 320 °C on the grain size of the solution-treated material is quite subtle. The optical micrographs also reveal that the microstructure is dominated by large continuous precipitates in the aged materials (Figures 1(b) and (c)). These precipitates are mainly located in the grain interiors but they can be also found at the grain boundaries (GBs).

Figure 2(a) shows the TD inverse pole figure (IPF) map of the solution-treated material. The {0001} pole figure (PF) in Figure 2(b), showing the orientations of the grains in the map, reveals that this plate exhibits the typical basal texture of rolled Mg alloys, where the basal planes are mainly parallel to the rolling plane.[5,6] In agreement, according to the IPFs in the TD calculated from XRD (Figures 2(c) through (e)) the solution-treated material (Figure 2(c)) displays a tendency for the TD to spread between the $\langle 10\bar{1}0\rangle$ and the $\langle 11\bar{2}0\rangle$ poles, which is consistent with the predominance of blue and green colors in the map. This means that for most of the grains, the TD is close to the prismatic crystallographic directions, so that twinning should be the main active deformation system under compression at RT along the TD. The IPFs in the TD of the aged 1 and the aged 2 specimens (Figures 2(d) and (e)) show that the basal planes of those grains with $\langle 11\bar{2}0\rangle$//TD are somewhat tilted towards the TD during aging. So, the texture of the aged samples is slightly different from that of the solution-treated one, which is consistent with the small variation of the average grain size during the thermal treatments (Figure 1).

The distribution of the particles in the aged 1 and aged 2 specimens are shown in Figure 3, where SEM images from the ND-RD sections are displayed. Note that, based on texture (Figures 2(d) and (e)), it can be assumed that the image plane is close to a matrix prismatic plane and thus perpendicular to those precipitates on basal planes. It can be seen that, continuous β-$Mg_{17}Al_{12}$ basal precipitate plates, seen as parallel needles or laths in the micrographs, dominate the microstructure and distribute uniformly within the grain interiors for both aging conditions. It can be noted that a few precipitates oriented approximately perpendicular to these plates are also present within the grains (see

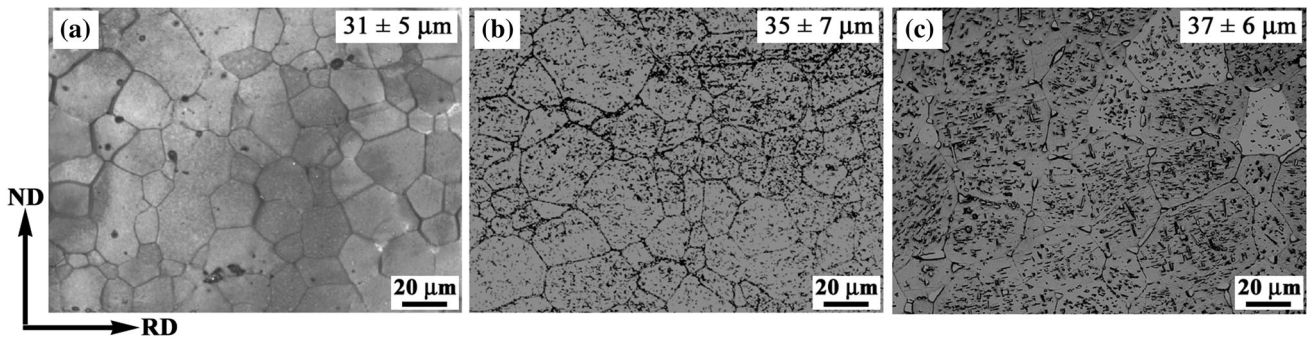

Fig. 1—Optical micrographs of the (*a*) solution-treated, (*b*) aged 1 and (c) aged 2 specimens. The average grain size values are included as insets in the micrographs.

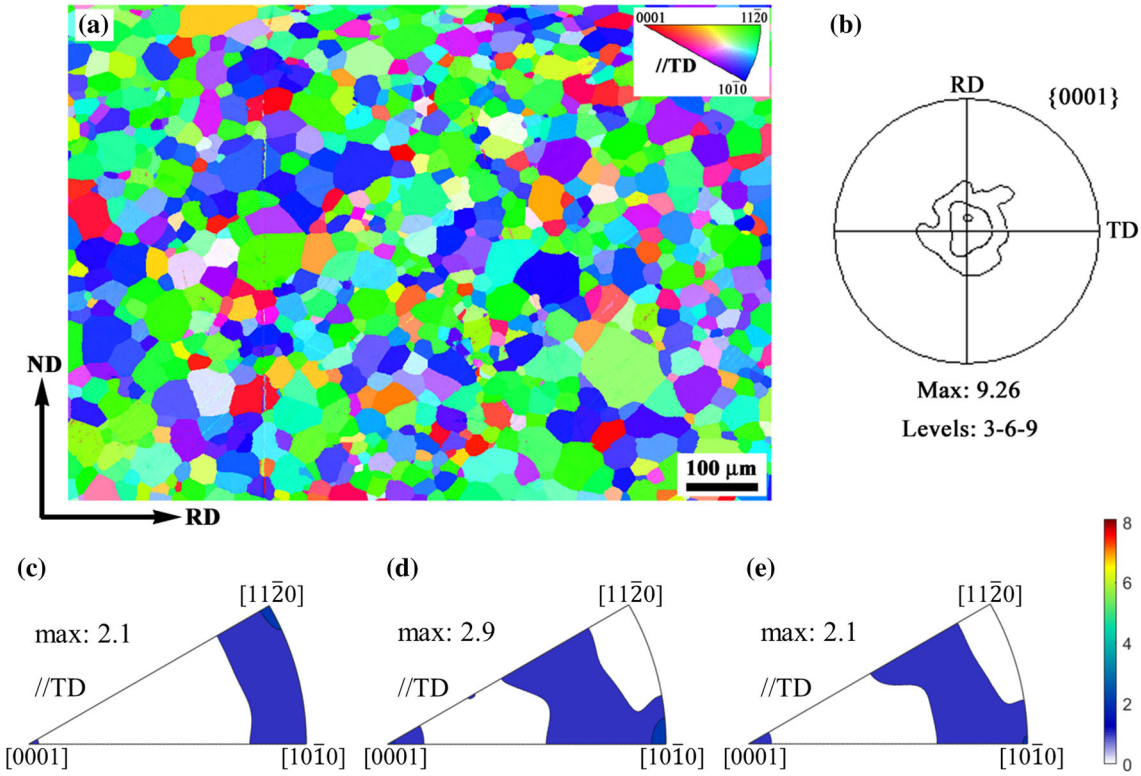

Fig. 2—(*a*) EBSD inverse pole figure (IPF) map of the solution-treated specimen and (*b*) {0001} pole figure showing the crystallographic orientations of the grains in (a). XRD IPFs in the transversal direction (TD) of the (*c*) solution-treated, (*d*) aged 1 and (*e*) aged 2 specimens.

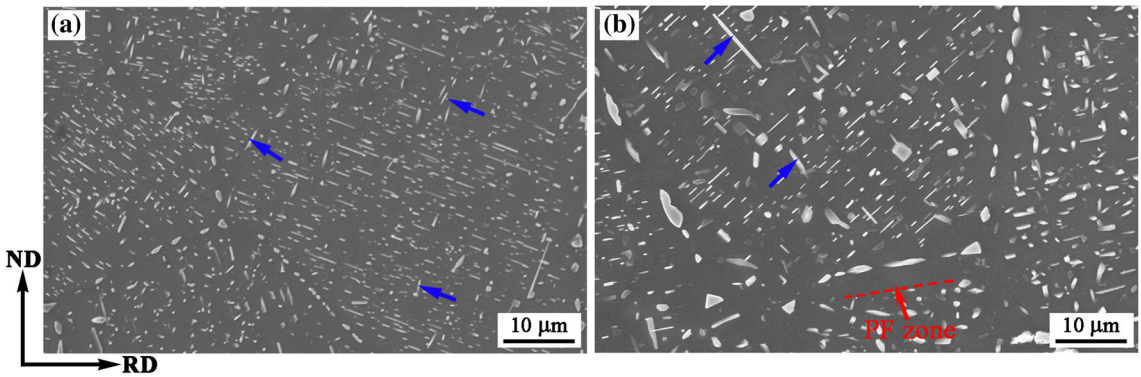

Fig. 3—SEM micrographs of the (*a*) aged 1 and (*b*) aged 2 specimens. The blue arrows identify the rod-shaped β precipitates, not considered in the present analysis, while the red arrow identify a precipitate-free (PF) zone adjacent to a grain boundary (Color figure online).

blue arrows). These have been identified as rod-shaped β precipitates, being their long axis aligned with the *c*-axis.[34,49] It should be mentioned that, for the present work, only the plated-shaped precipitates will be considered.

It is also patent from Figure 3 that precipitation during aging also takes place at the GBs. In this way, particles decorating the GBs are observed in both aged specimens, especially after aging for 116 hours (Figure 3(b)). Such particles could effectively pin the GBs, so that they would restrict grain growth during the aging treatments at 320 °C. Precipitate-free zones (PFZs) are present in the vicinity of the GBs, again especially noticeable in the specimen aged for 116 hours (see red arrow in Figure 3(b)). These may form by (i) a reduction of the solute content in the regions close to the GBs caused by the growth of the GB precipitates during aging and (ii) a reduction during the water-quenching following the solution treatment of the vacant content in these regions and thus of nucleating sites for the precipitates.[47] Since the PFZs are mainly formed on extended aging times, the former is the most likely mechanism.

From the calculated ternary phase diagram using the PANDAT software, the volume fraction of precipitates was estimated to be only 1.7 pct for both aging conditions. However, by eye, precipitates are much larger in the aged 2 (Figure 3(b)) than in the aged 1

(Figure 3(a)) condition, so that they form denser layers, closer to lamellar structures, in the former than in the latter. For a more accurate comparison, the dimensions of the individual basal plates were quantitatively determined from the SEM micrographs (Table I). The mean plate thickness (t_t) was calculated as the average height of the above-mentioned laths, which corresponds to the intersection of the basal plates with the matrix prismatic planes. For the calculation of the mean plate diameter (d_t), it was taken into account that the $Mg_{17}Al_{12}$ basal plates are actually parallelograms whose long axes are parallel to the three close packed orientations of the matrix.[45] To simplify the analysis, the precipitate shape was approximated to basal discs whose mean diameter is equal to the average length of the largest laths in the pictures. For each aged condition, ~ 145 and ~ 540 measurements were made for the calculation of t_t and d_t, respectively. As detailed in Table I, after annealing at 320 °C for 2 hours, the basal plates have a mean diameter of 3.42 ± 0.79 μm and a mean thickness of 0.15 ± 0.06 μm. With increasing the aging time to 116 h, the plates grow in both diameter and thickness, their aspect ratio (d_t/t_t) being higher for the aged 1 than for the aged 2 specimen.

B. *Mechanical Behavior*

Examples of compression curves for the AZ80 alloy tested along the TD in the solution-treated, aged 1 and aged 2 conditions can be seen in Figure 4(a). The three curves exhibit the typical concave-up shape associated with the predominance of tensile twinning during the first stages of deformation,[23] the yield point reaching an average value of about 95 MPa for the solution-treated specimen and of 105 MPa for the two aged specimens. According to the familiar Hall–Petch relationship, the subtle increase in the mean grain size during aging (Figure 1) would lead to an insignificant decreased yield stress in the aged samples compared to the solution-treated one. Similarly, a slightly higher activity of basal slip in the aged samples promoted by the tilt of the c-axes from the ND towards the TD in a few grains during aging (Figures 2(c) through (e)) would always result if anything in a small decrease of the yield stress. Finally, the large presence of solutes in solid solution in the aged samples cannot explain the increase of the yield stress after aging either. The contribution of the solid solution to the yield stress can be calculated as

$$YS_{ss} = CX^{2/3} \quad [1]$$

where C = 197 MPa and X is the atomic fraction of solute.[50,51] Using the JMat Pro software, the solute atomic fraction was estimated to be 0.0681 before aging and 0.0589 after aging. Substituting these values in Eq. [1], the yield stress of the solution-treated condition was estimated to decrease by 3 MPa due to the solute loss upon aging.

Therefore, the increase of the compressive yield stress (CYS) along the TD on aging can be only attributed to the precipitation of the $Mg_{17}Al_{12}$ basal plates. However, precipitates lead to only 10 MPa of maximum hardening, while previous works on Mg-Al-Zn alloys[29,31,33,35,36,41] show that the yield stress in twinning-dominating conditions can be increased by ~ 100 MPa upon continuous precipitation. This is mainly due to the fact that in the present study, the aging treatments were carried out at higher temperature, which results in a lower precipitate volume fraction of larger-sized precipitates and thus in a lower strengthening efficiency. However, the increased grain size, the tilt of the c-axis towards the TD or the solute loss, could contribute to the small overall strengthening of the alloy on aging. It is also worth-noting that, despite the different precipitate distribution observed in the aged 1 (Figure 3(a))

Table I. Mean Diameter (d_t), Thickness (t_t), and Aspect Ratio ($AR = d_t/t_t$) of the Basal Plates in the Aged Specimens

Aging Time (h)	d_t (μm)	t_t (μm)	$AR = d_t/t_t$
2	3.42 ± 0.79	0.15 ± 0.06	23.56
116	3.64 ± 0.91	0.27 ± 0.10	13.43

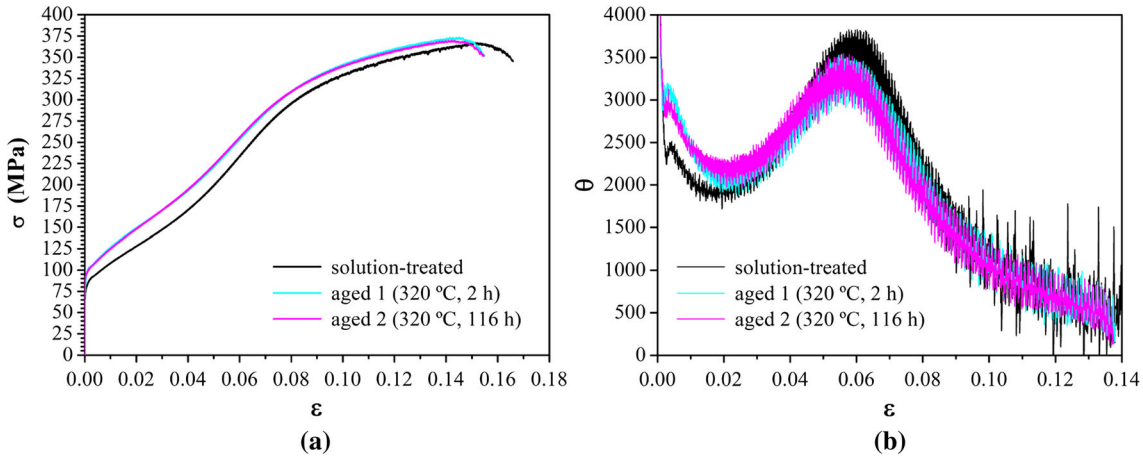

Fig. 4—Mechanical behavior at room temperature of the solution-treated, aged 1 and aged 2 specimens under compression along the transversal direction. (*a*) True stress *vs* true strain and (*b*) work hardening rate *vs* true strain.

and aged 2 (Figure 3(b)) specimens, strengthening is nearly identical for both specimens, which is consistent with the hardness Vickers measurements.

In agreement with the true stress-true strain response, the work hardening rate curves of the solution-treated and aged materials (Figure 4(b)) exhibit a distinct maximum at an intermediate strain. This is typically observed when twinning dominates deformation and is usually associated to a rapid increase of stress to activate pyramidal ⟨c + a⟩ slip after the exhaustion of twinning.[52] However, after the initial drastic decrease observed at very low strains, ascribed to the elastic-plastic transition, the work hardening rate exhibits another much smaller maximum for the three specimens. This is consistent with a sequential activation of deformation modes during the first stages of deformation and could indicate that a small fraction of grains begin to deform plastically by basal slip whilst those grains suitably oriented for twinning continue to keep deforming elastically up the macroscopic yield stress, where all grains deform plastically.

C. *Characterization of Deformed Microstructures*

Figures 5(a) through (c) illustrate the IPFs in the compressive direction (CD) calculated from XRD of the solution-treated, aged 1 and aged 2 materials compressed to 5 pct engineering strain. It can be seen that these three deformation textures are qualitatively similar to each other, but there is a marked difference with the textures of the undeformed materials (Figures 2(c) through (e)). In particular, it is clear that compression along the TD causes a large tilt of the *c*-axes, initially close to the ND of the rolled sheet, to become approximately aligned with the CD. This is consistent with the rapid 86 deg reorientation of the ⟨0001⟩ axis promoted by twinning. In agreement, the CD IPF maps from sections perpendicular to the CD of these samples (Figures 5(d) through (f)) show clear twins and a profuse amount of material colored in red tones.

Quantifications from the XRD data of the increase in the volume fraction of material with its ⟨0001⟩ axis parallel to the TD (max deviation = 20 deg) revealed that the volume fraction of twins decreases significantly in the aged 1 condition (Figure 5(b)) compared to the solution-treated one (Figure 5(a)). In contrast, the twin fraction is only slightly lower in the aged 2 condition (Figure 5(c)) than in the solution-treated one (Figure 5(a)). The slight tilt of the *c*-axes from the ND to the TD experienced by a few grains in the solution-treated sample during aging (Figures 2(c) through (e)) could lead to a reduced activity of twinning in the aged samples compared to the solution-treated condition caused by a promotion of basal slip. However, given that the texture change is nearly identical during both aging treatments (Figures 2(d) and (e)), the decrease of the volume fraction of twins after compression should be also very similar in both aged specimens, but they are very different (Figures 5(b) and (c)). This indicates that the changes in texture caused by aging have a minor effect in the decreased twinning activity in the aged specimens.

A decrease in the volume fraction of twinning compared with the un-aged condition was also reported by Jain *et al.*[29] for a weakly textured AZ80 alloy with a uniform distribution of mainly continuous precipitates

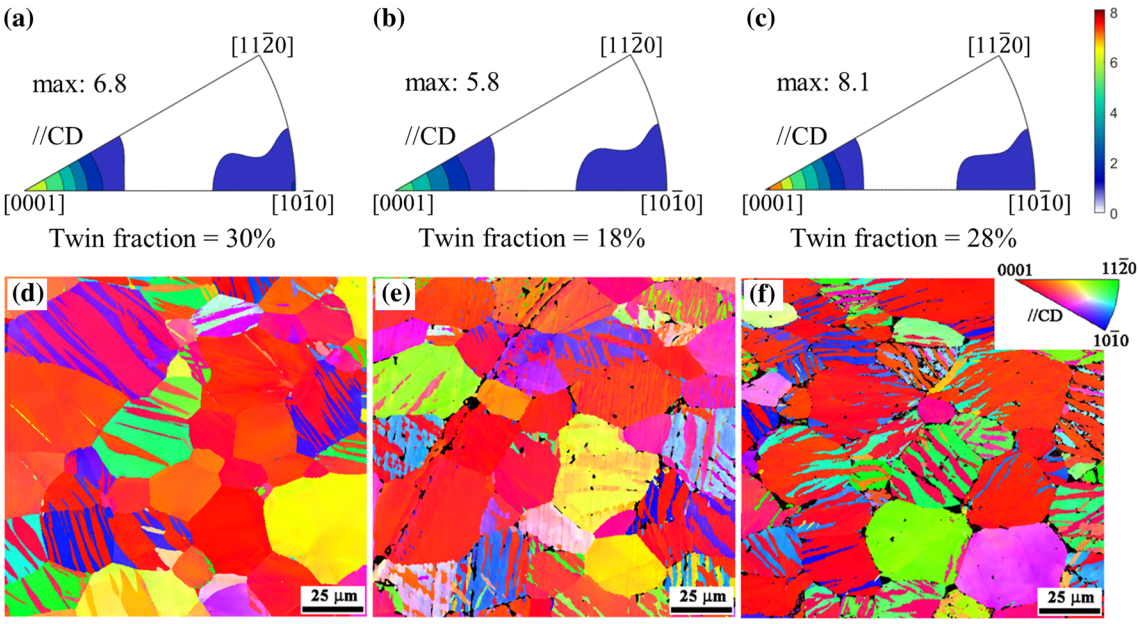

Fig. 5—Orientation data of specimens compressed to 5 pct engineering strain along the transversal direction. (*a* to *c*) XRD inverse pole figures (IPFs) in the compressive direction (CD) and (*d* to *f*) EBSD IPFs maps from sections perpendicular to the CD of the (a, d) solution-treated, (b, e) aged 1 and (c, f) aged 2 conditions. (a to c) The non-indexing points in (d) through (f) are shown as black pixels.

attributable to a decreased activity of twinning. In contrast, aging an extruded AZ91 alloy showing a dense population of lamellar plate-shaped particles[35] and a rolled AZ91 alloy containing both discontinuous and continuous $Mg_{17}Al_{12}$ precipitates[41] showed to have significantly increased yield stress, but unchanged twin volume fraction when testing in twinning dominated conditions. This suggests that the activity of twinning and thus the volume fraction of twins in the aged samples is mainly determined by the particle distribution.

SEM inspections (Figures 6(a) through (c), (e), and (f)) confirm the profusion of twinning in the solution-treated and the aged samples upon compression along the TD. Assuming to be comparable to the area fraction of twins, the volume fraction of twins (f_{twin}) was manually measured from SEM micrographs on sections perpendicular to the CD by means of a point counting analysis with a squared net. A minimum of four micrographs per condition were used, being more than 500 points per micrograph counted. The number of twins per unit area (N_{twin}) of the three samples was calculated by counting manually the number of twins on the same pictures. The results (Figure 6(d)) verify that f_{twin} is lower in the aged samples, especially the aged 1, than in the solution-treated sample. On the contrary, N_{twin} is much higher in the aged samples, especially the aged 1, than in the solution-treated sample. This suggests that, as previously observed in binary Mg alloys,[28–30,35,40] twins are thinner, but more numerous in the aged specimens than in the solution-treated condition. This, in turn, suggests that twins can be formed without trouble in alloys containing precipitates, even in the presence of a large amount of particles at the GBs, but their growth is limited. It has been proposed[28,30,36] that, since stress relaxation is a driving force behind twin propagation and growth,[53] when the growth of twins is hindered, the stress undergone by the grain is higher because the twin cannot accommodate the imposed strain. So, new twins have to nucleate within the grain for the plastic strain by twinning to proceed. This hypothesis has been recently proved by means of molecular dynamic simulations.[54]

Closer SEM inspections of the aged specimens on sections perpendicular to the CD (Figure 6(e)), where twin traces are relatively aligned with the plates, reveal that particles are able to pin the twin boundaries, hindering their lateral growth, or simply act as obstacles which prevent the growing twins from merging and consuming entire grains. This way, twins appear to become somewhat sandwiched between the basal precipitate plates, which arrange to form parallel layers. So, twinning growth and thus twin thickness seems to be affected by the interparticle spacing in the *c*-axis direction. On the other hand, SEM inspections on sections parallel to the CD (Figure 6(f)), where twin traces are inclined towards the basal precipitate plates, show that particles are mostly embedded by growing twins with no evidence of shearing.

IV. DISCUSSION

Our results reveal an increase of about 10 MPa in the CYS along the TD after aging at 320 °C for as much 2 hours as 116 hours in relation to the solution-treated condition (Figure 4(a)). This increase of the CYS was mainly attributed to the precipitation of the $Mg_{17}Al_{12}$

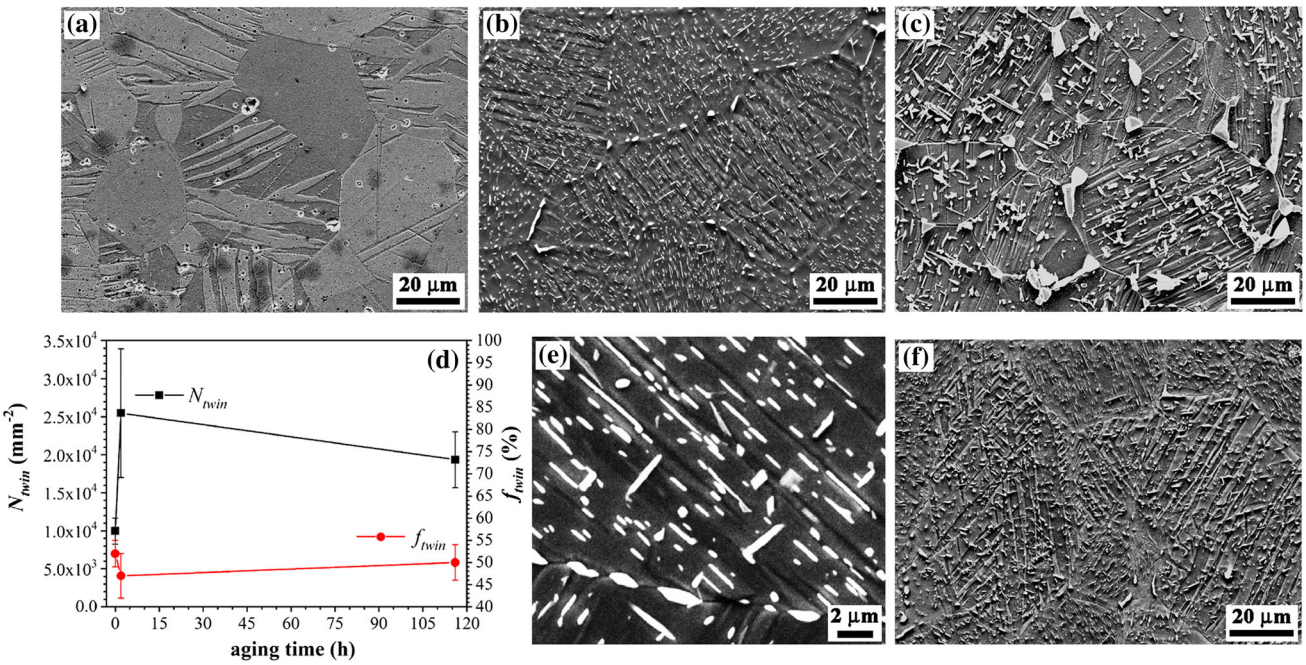

Fig. 6—Results of SEM inspections on specimens deformed in compression up to an engineering strain of 5%. (*a* to *c*, *e*, *f*) Micrographs from sections perpendicular (a to c, e) and parallel (f) to the compressive direction of the (*a*) solution-treated, (b, e, f) aged 1 and (c) aged 2 conditions. (d) Representation of the number density (N_{twin}) and the volume fraction (f_{twin}) of twins as a function of the aging time.

basal plates. More specifically, it could be attributed to the preferential strengthening effect of such precipitate plates on extension twinning ($K_1 = \{10\bar{1}0\}$), which according to the shape of the compressive (Figure 4(a)) and the work hardening rate curves (Figure 4(b)), is the main active deformation mechanism under compression along the TD for the three thermal conditions. Precipitates have been proved to effectively hinder twin growth, in such a way that twins are more numerous, but generally thinner in the aged than in the solution-treated condition (Figure 6(d)). One interesting observation is that, despite the difference in the precipitate distribution between the aged 1 and aged 2 specimens (Figure 3), both samples exhibit the same rise of the CYS in relation to the solution-treated condition (Figure 4(a)).

The $CRSS_{twinning}$ values were approximated as CYS $\times$ SF, where SF is the average Schmid factor for the twin system (approximately equal to 0.4, according to the calculations made using the HKL software).[38] Afterwards, the increment of $CRSS_{twinning}$ due to precipitation was estimated to be about 5 MPa for both the aged 1 and aged 2 conditions, which is a very modest strengthening effect. However, it is also clear that the particles have had an effect on the twin volume fraction and number density (Figures 5(a) through (c) and 6(d)). Furthermore, as already noted, when viewed in the section perpendicular to the CD, it is clear that the width of the twins is often constrained between bands of particles (Figure 6(e)).

The crystallography is such that the twinning planes on which the SF is a maximum intersect the observation plane to produce a line that lies on the precipitate habit plane. The twin will thicken, attempting to maintain its invariant K_1 plane until it encounters sufficient obstacles (particles) that it becomes arrested. In contrast to a high angle boundary, the twin boundary cannot curve arbitrarily without an additional energy penalty associated with deviation from the K_1 plane. Therefore, unlike in Zener pinning of a general high angle boundary, we do not observe bulging of the twin boundary in the gaps between precipitates, even when the gap is large.

The ability to calculate the precipitation strengthening of twinning is a critical requirement in designing Mg alloys with improved mechanical properties. However, despite a number of recent studies,[28,30,31,33,36,40,41,43] there is not yet a proven method for performing such calculations. Indeed, it is not yet clear which particle parameters are important to consider.

Several approaches have been used to estimate the increase of the CRSS for twin growth caused by precipitation. The first is to simply apply the standard Orowan equation developed for slip to calculate the bowing stress required for a single twinning dislocation. These calculations tend to underestimate the measured strengthening effect by around 5 to 10 times.[28,30–32,36,40,43]

The second method is to assume that the additional back-stress caused by the twinned material surrounding an unsheared precipitate is the dominant contribution. However, calculations based on assuming a fully elastic accommodation of the misfit that leads to the back-stress, tend to overestimate the strengthening effect by an order of magnitude.[31,36]

To account for plastic relaxation of this additional back-stress, it has been proposed that the additional stress required for basal slip to occur within the twin is the important factor, supposing that this will provide a reasonable estimate of the increase in back-stress that cannot be plastically relaxed. Such calculations have been shown to give reasonable agreement with the measured strengthening increment, but are not based on a mechanistic understanding of the interaction between twins and precipitates.[31,36,43]

More recently, Barnett[48] has calculated the strengthening effect based on treating the twin front as a super-dislocation (which consists of multiple twinning dislocations) and estimating the stress required to bow this super-dislocation. This recognizes that there is a minimum twin thickness that is able to propagate and for a twin to propagate around and beyond a particle would necessarily involve bowing of multiple twinning dislocations. This calculation also gives a reasonable agreement with the experimental strengthening.

The calculation method used will not only give a different prediction of strengthening effect, but will also give a different dependency on particle parameters (*e.g.*, volume fraction, size, and spacing). None of the calculations are based on a careful consideration of the all physical processes that can occur when a twin encounters a precipitate. We have used all of these approaches to calculate the strengthening effect in the present case and compared the results to our measurements.

A. *Orowan Strengthening*

Since the precipitates formed in the present AZ80 Mg alloy during aging at 320 °C are engulfed by twins without shearing (Figure 6(f)), the following expression, based on the Orowan model, was used to calculate the increment of $CRSS_{twinning}$ due to precipitate strengthening ($\Delta\tau_{twin}$)

$$\Delta\tau_{twin} = \frac{G_{Mg} b_{Mg}}{2\pi\lambda_{twin}\sqrt{1-\nu_{Mg}}} \ln\left(\frac{D_p^{twin}}{r_{Mg}^{twin}}\right) \qquad [2]$$

where $G_{Mg} = 16.5$ GPa is the shear modulus of the Mg matrix, b_{Mg} is the magnitude of the Burgers vector for the twinning dislocations in Mg, λ_{twin} is the effective planar interparticle spacing on the twin plane, $\nu_{Mg} = 0.35$ is the Poisson's ratio of the Mg matrix, D_p^{twin} is the mean planar diameter of the particles on the twin plane and r_{Mg}^{twin} is the core radius of the twinning dislocations in Mg.

Based on a previous study of the present authors,[43] the Burgers vector and the core radius of twinning dislocations in Mg were assumed to be 0.46 Å and 0.96 nm, respectively. However, the appropriate values of λ_{twin} and D_p^{twin} were determined using the measured particle dimensions (Table I). The effective planar

interparticle spacing on the twin plane was found by initially determining the mean planar center-to-center interparticle spacing on such plane, given by $1/\sqrt{N_a^{twin}}$, where N_a^{twin} is the number of particles per unit area of twin plane. To do this, Fullman's method,[55] assuming a regular array of particles, was followed. So, the probability of intersecting a single basal plate by a twin plane (P_{twin}) was calculated as $d_t \sin\theta + t_t \cos\theta$,[31] where $\theta = 43.2$ deg is the angle between the twin plane and the basal plates. Then, N_a^{twin} was approximated by $N_v \times P_{twin}$, where $N_v = f/V_p$ is the number of particles per unit volume, f representing the volume fraction of particles and V_p the mean volume of individual particles $\left(=\frac{\pi}{4} d_t^2 t_t\right)$. Finally, the effective planar interparticle spacing, schematically shown in Figure 7(b), was estimated as

$$\lambda_{twin} = \frac{1}{\sqrt{N_a^{twin}}} - D_p^{twin} \quad [3]$$

where D_p^{twin} is the mean planar diameter of the particles on the twin plane and was also found following the analysis of Fullman.[55] As shown in Figure 7(a), random intersection of a basal plate with the twin plane will produce a rectangular cross-section of mean length $d_p^{twin} = \pi d_t/4$ and mean width $t_p^{twin} = t_t/\sin\theta$. The mean planar diameter of particles is found by determining the average value of the precipitate dimension which is parallel to the direction of the gap to be bowed by dislocations.[36] Assuming that dislocations on the twin plane have to go through the length of the above-mentioned rectangles before circumventing them (Figure 7(b)), the mean planar diameter of the particles on the twin plane was calculated as

$$D_p^{twin} = d_p^{twin} = \frac{\pi}{4} d_t \quad [4]$$

The calculated values of D_p^{twin}, λ_{twin} and $\Delta\tau_{twin}$ for the aged 1 and aged 2 specimens are compiled in Table II. It can be seen that λ_{twin} is lower for the aged 1 than for the aged 2 condition, which is consistent with the observed particle coarsening with increasing the annealing time (Table I). As a consequence, unlike the CYS, which remains the same for both aged conditions, $\Delta\tau_{twin}$ is higher for the peak-aged than for the over-aged specimen.

B. *Back-Stress*

The other contribution to the increase of the CRSS for twin growth derives from the additional back-stress on the twin generated by unsheared particles.[31,36] When precipitates are not sheared in the twinned material a plastic strain discontinuity occurs at the interface between the particle and the twin.[55] This is an additional contribution to the overall back-stress, which must be relieved by elastic and/or plastic deformation for the twin to keep growing without particles.

The back-stress generated by particles can be calculated as the shear stress component on the basal plane within the twin.[31] In particular, the back-stress (σ_b) for basal plates is given by

$$\sigma_b = Gf(0.10) \quad [5]$$

According to this expression, the back-stress for the precipitate fraction formed in the AZ80 Mg alloy during aging at 320 °C (1.7 pct) takes a value of 28 MPa. Since this depends only on the volume fraction of precipitates, but not on their size or spacing, it is the same for both the aged 1 and the aged 2 specimens, which is consistent with the invariability of the CYS with the aging time. However, this value exceeds the expected critical resolved shear stresses for basal and prismatic slip,[56]

Table II. Mean Planar Diameter of the Basal Plates on the Twin Plane $\left(D_p^{twin}\right)$, Effective Planar Interparticle Spacing on the Twin Plane (λ_{twin}) and Orowan Strengthening Against Twinning ($\Delta\tau_{twin}$) of the Aged Specimens

Aging Time (h)	D_p^{twin} (μm)	λ_{twin} (μm)	$\Delta\tau_{twin}$ (MPa)
2	2.68	2.97	0.40
116	2.86	5.00	0.24

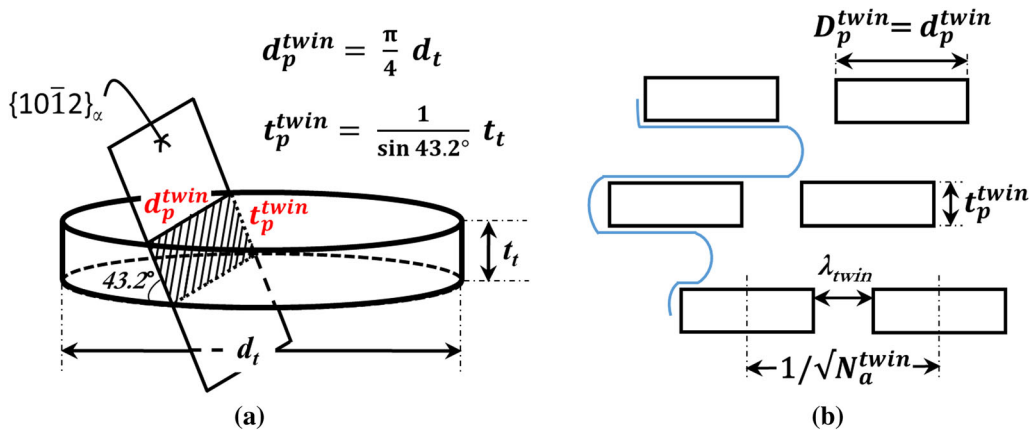

Fig. 7—Schematic showing the (*a*) intersection area of the basal plates with twin planes and (*b*) the effective planar interparticle spacing (λ_{twin}) as well as the interception of particles by dislocations on twin planes.

being an order of magnitude higher than that obtained by multiplying the measured CYS by the SF for the twin system. This indicates that the stress incompatibility cannot be accommodated elastically alone, but must also be accommodated plastically.[31,36] This is consistent with the high density of dislocations experimentally observed by Gharghouri *et al.*[46] around the unsheared particles within the twins.

C. *Basal Slip in the Twin*

It is likely that the plastic deformation required to attenuate the large elastic stresses that would otherwise arise as described above[31,36] takes place by basal slip. This is because the smallest CRSS of all the slip systems corresponds to basal slip. Moreover, the lattice in the twin is favorably oriented for basal slip.[36] This is because, due to the reorientation of the lattice caused by twinning, the basal planes, which are approximately parallel to the CD in the parent material, form ~ 86 deg with the CD in the twin.

The precipitation strengthening of the basal slip in the twin ($\Delta\tau_{basal(twin)}$) can be calculated by the Orowan model, considering precipitates now engulfed in the twinned material. For this purpose, the magnitude of the Burgers vector and the core radius of basal dislocations in Mg (0.32 nm for both parameters[43]) were considered. Moreover, the appropriate values of the effective planar interparticle spacing on the basal plane in the twin ($\lambda_{basal(twin)}$) as well as the mean planar diameter of the particles on the same plane $\left(D_p^{basal(twin)}\right)$ were determined taking into account that, since the matrix is rotated by twinning, the parent-basal plates are nearly parallel to one set of parallel prismatic planes in the twin.[31,36]

Table III lists the estimated values of $D_p^{basal(twin)}$, $\lambda_{basal(twin)}$ and $\Delta\tau_{basal(twin)}$ for the aged specimens. Note that, since the cross-sections of the parent-basal plates with both the twin plane (Figure 7(a)) and the basal plane within the twin (Figure 8(a)) is a rectangle with the same length ($= \pi d_t/4$), D_p^{twin} (Table II) and $D_p^{basal(twin)}$ exhibit the same values for both aging conditions. However, $\lambda_{basal(twin)}$ (schematically shown in Figure 8(b)) is lower than λ_{twin} (Table II) as much for the aged 1 as for the aged 2 condition, which could be attributed to a higher probability of the parent-basal plates being intersected by a single basal plane within the twin ($P_{basal(twin)} = 0.99d_t + 0.07t_t$) than by a single twin plane ($P_{twin} = 0.68d_t + 0.73t_t$).

D. *Bowing of Super-Dislocation*

Barnett[48] has recently presented a calculation for the bowing stress around obstacles considering the twin front as a super-dislocation, which consists of multiple twinning dislocations. This accounts for the fact that the bowing of a single twinning dislocation is not sufficient to enable the twin to propagate beyond the particle, since there is a minimum twin thickness that leads to growth for a given imposed shear stress.

Table III. Mean Planar Diameter of the Parent-Basal Plates on the Basal Plane in the Twin $\left(D_p^{basal(twin)}\right)$, Effective Planar Interparticle Spacing on the Basal Plane in the Twin ($\lambda_{basal(twin)}$) and Orowan Strengthening Against Basal Slip in the Twin ($\Delta\tau_{basal(twin)}$) of the Aged Specimens

Aging Time (h)	$D_p^{basal(twin)}$ (μm)	$\lambda_{basal(twin)}$ (μm)	$\Delta\tau_{basal(twin)}$ (MPa)
2	2.68	2.10	4.48
116	2.86	3.89	2.43

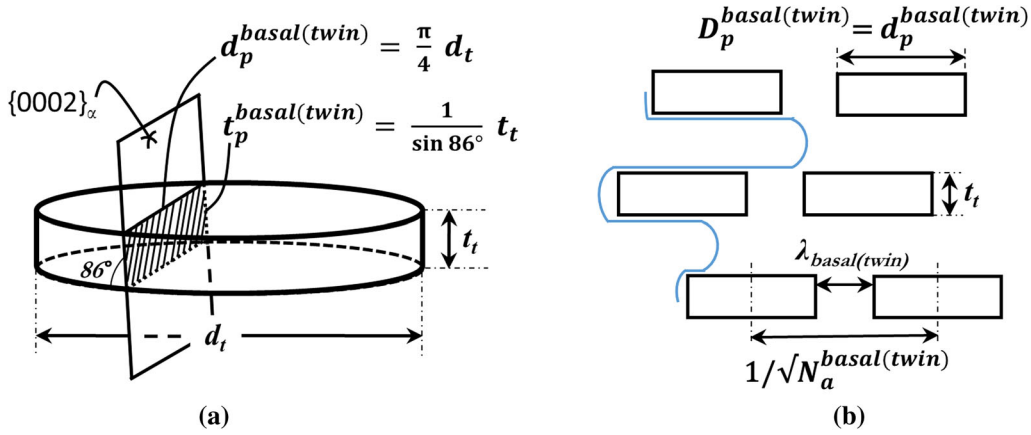

Fig. 8—Schematic showing the (*a*) intersection area of the parent-basal plates with basal planes within the twin and (*b*) the effective planar interparticle spacing ($\lambda_{basal(twin)}$) as well as the interception of particles by dislocations on basal planes within the twin.

Table IV. Calculated Strengthening Effect of Particles (MPa) on the Critical Resolved Shear Stress for Twin Growth Using Four Alternative Methods, Compared with the Value Derived from measurements

Aging Time (h)	Orowan (Single Dislocation)	Back-stress	Basal Slip in Twin	Orowan (Super-Dislocation)	Measured
2	0.40	28	4.48	9.27	5
116	0.24	28	2.43	5.51	5

We applied Barnett's approach[48] to calculate the bowing stress for the super-dislocation in the present case, obtaining a value of 42 MPa (assuming twin growth dominated yield and using SF = 0.4, as before). For twin growth to be energetically possible at this applied stress level, Barnett's analysis yields the minimum number of twinning dislocations in the expanding super-dislocation loop as approximately 114. This corresponds to a twin thickness of approximately 43 nm.

To bow this super-dislocation, taking the mean particle spacings on the twinning plane derived previously (3 and 5 μm for aged 1 and aged 2 conditions, respectively), requires stress of approximately 9.27 and 5.51 MPa, respectively.

E. *Comparison of Calculation Methods*

The strengthening against twin growth calculated by the four methods above was compared with that determined from measurement, as shown in Table IV. Firstly, it can be seen that there is 2 order of magnitude difference between the highest and the lowest calculated value, based on the method used. Such a discrepancy serves to highlight the problem in using such calculations to aid alloy design. Two of the methods provide very good estimates of the of the CRSS increase for twin growth: the model based on basal slip in the twin, especially accurate for the aged 1 condition and the model based on the bowing of super-dislocations, especially accurate for the aged 2 condition. So, the interaction between propagating twins and particles still remains an unclear phenomenon, but seems to be related to the particle distribution. This is consistent with the different volume fraction of twins observed in the two aged samples after testing (Figures 5(a) through (c) and Figure 6(d)).

For the aged 1 specimen, the calculation method that gives a strengthening estimate closest to the measured value is the Orowan stress necessary to bow basal dislocations in the twin. The physical justification for this calculation is that by inhibiting dislocation motion in the twin, the extent of plastic relaxation will be reduced. Whilst a rigorous calculation of plastic relaxation is complex,[53] and this approach is certainly a great over-simplification, the present results confirm that this metric may be useful in estimating the magnitude of the strengthening effect. It has also been previously demonstrated to correctly capture the trends regarding the effect of the shape and habit of particles on the strengthening of the twinning system.[31] This calculation is based on the assumption that the extent to which plastic relaxation is affected by precipitation is most critical in determining the strengthening effect. However, this approach does not imply a mechanism by which the twins negotiate the particles because no matter how an unsheared particle ends up embedded in sheared (twinned) material, the same back-stress and plastic relaxation is expected.

For aged 2 specimen (containing lamellar-type precipitates), the calculation method that gives a strengthening estimate closest to the measured value is the stress required to bow a twinning super-dislocation loop capable of further expansion. An important distinction between this method and the strengthening of the basal slip in the twin is that it entails a mechanism by which the twins propagate through a microstructure containing unsheared precipitates (and do so relatively easily). Inevitably, in an alloy with a significant precipitate volume fraction, twins must inevitably engulf particles if they are to grow. As argued by Barnett,[48] this cannot occur by bowing of a single twinning dislocation for energetic reason, but involves the thickening of the twin sufficiently to bypass the particle. However, plastic relaxation effects were not considered when calculating the stress required to bow the propagating super-dislocation between particles.

V. CONCLUSIONS

A cast AZ80 Mg alloy was homogenized and hot rolled in order to obtain a plate with the basal planes aligned with the rolling plane. The rolled plate was solution-treated and aged at 320 °C for 2 or 116 hours. Then, the solution-treated and the aged materials were tested in compression at room temperature along the transverse direction. A detailed characterization of particles and twins was accomplished by scanning electron microscopy. The effect of the precipitate basal plates on the strength of the alloy was estimated by using different models, these predictions being compared against the experimental mechanical properties. The conclusions that can be extracted from this work are:

1. The compressive yield stress increases by about 10 MPa after aging up to both the aged states. This yield stress increase can be ascribed to the precipitation strengthening of twinning, the main active deformation mechanism.
2. A higher number of thinner twins are observed in the aged samples, suggesting that precipitation promotes twin nucleation, but inhibits twin growth. So, the precipitation strengthening of twinning is mainly determined by the additional stress required for the twins to grow.
3. Four alternative methods have been applied to estimate the increase of the critical resolved shear

stress for twin growth and compared with the measured strengthening. These calculation methods give 2 orders of magnitude difference in estimated strengthening effect, spanning the measured value. Two different metrics approximates to the measured strength increment depending on the aging time: the Orowan stress necessary to bow basal dislocations in the twin and the Orowan stress to bow super-dislocations loops capable of further expansion. So, the strengthening effect of particles on twinning seems to be determined by the particle distribution.

ACKNOWLEDGMENTS

The authors are grateful to the EPSRC LATEST2 program grant (EP/H020047/1) for funding. Thanks also to D. Strong from the University of Manchester for technical support. This research was undertaken in the facilities of the School of Materials in the University of Manchester, including the Electron Microscopy Center. The data presented in this paper may be obtained by contacting the corresponding author.

OPEN ACCESS

REFERENCES

1. I.J. Polmear: *Mater. Sci. Tech.*, 1994, vol. 10, pp. 1–16.
2. B.L. Mordike and T. Ebert: *Mater. Sci. Eng. A*, 2001, vol. 302, pp. 37–45.
3. M. Hakamada, T. Furuta, Y. Chino, Y. Chen, H. Kusuda, and M. Mabuchi: *Energy*, 2007, vol. 32, pp. 1352–60.
4. M. Easton, A. Beer, M. Barnett, C. Davies, G. Dunlop, Y. Durandet, S. Blacket, T. Hilditch, and P. Beggs: *JOM*, 2008, vol. 60, pp. 57–62.
5. I.L. Dillamore and W.T. Roberts: *Metall. Rev.*, 1965, vol. 10, pp. 271–380.
6. Y.N. Wang and J.C. Huang: *Mater. Chem. Phys.*, 2003, vol. 81, pp. 11–26.
7. J.W. Christian and S. Mahajan: *Prog. Mater. Sci.*, 1995, vol. 39, pp. 1–157.
8. I. Ulacia, N.V. Dudamell, F. Gálvez, S. Yi, M.T. Pérez-Prado, and I. Hurtado: *Acta Mater.*, 2010, vol. 58, pp. 2988–98.
9. M.R. Barnett: *Metall. Mater. Trans. A*, 2003, vol. 34A, pp. 1799–806.
10. H. Watanabe and K. Ishikawa: *Mater. Sci. Eng. A*, 2009, vol. 523, pp. 304–11.
11. J. Bohlen, P. Dobroň, J. Swiostek, D. Letzig, F. Chmelík, P. Lukáč, and K.U. Kainer: *Mater. Sci. Eng. A*, 2007, vol. 462, pp. 302–06.
12. T. Al-Samman, X. Li, and S.G. Chowdhury: *Mater. Sci. Eng. A*, 2010, vol. 527, pp. 3450–63.
13. E.A. Ball and P.B. Prangnell: *Scripta Metall. Mater.*, 1994, vol. 31, pp. 111–16.
14. J. Bohlen, M.R. Nürnberg, J.W. Senn, D. Letzig, and S.R. Agnew: *Acta Mater.*, 2007, vol. 55, pp. 2101–12.
15. L.W.F. Mackenzie, B. Davis, F.J. Humphreys, and G.W. Lorimer: *Mater. Sci. Technol.*, 2007, vol. 23, pp. 1173–80.
16. N. Stanford and M.R. Barnett: *Mater. Sci. Eng. A*, 2008, vol. 496, pp. 399–408.
17. J.D. Robson: *Metall. Mater. Trans. A*, 2014, vol. 45A, pp. 3205–12.
18. M.R. Barnett, M.D. Nave, and C.J. Bettles: *Mater. Sci. Eng. A*, 2004, vol. 386, pp. 205–11.
19. N. Stanford and M.R. Barnett: *J. Alloys Compd.*, 2008, vol. 466, pp. 182–88.
20. C. Xu, T. Nakata, X.G. Qiao, H.S. Jiang, W.T. Sun, Y.C. Chi, M.Y. Zheng, and S. Kamado: *Mater. Sci. Eng. A*, 2017, vol. 685, pp. 159–67.
21. S. Suwas, G. Gottstein, and R. Kumar: *Mater. Sci. Eng. A*, 2007, vol. 471, pp. 1–14.
22. J. He, B. Jiang, X. Yu, J. Xu, Z. Jiang, B. Liu, and F. Pan: *J. Alloys Compd.*, 2017, vol. 698, pp. 771–85.
23. M.R. Barnett, Z. Keshavarz, A.G. Beer, and D. Atwell: *Acta Mater.*, 2004, vol. 52, pp. 5093–5103.
24. A. Ghaderi and M. Barnett: *Acta Mater.*, 2011, vol. 59, pp. 7824–39.
25. N. Stanford and M.R. Barnett: *Int. J. Plast.*, 2013, vol. 47, pp. 165–81.
26. V. Herrera-Solaz, P. Hidalgo-Manrique, M.T. Pérez-Prado, D. Letzig, J. Llorca, and J. Segurado: *Mater. Lett.*, 2014, vol. 128, pp. 199–203.
27. J.F. Nie: *Scripta Mater.*, 2003, vol. 48, pp. 1009–15.
28. N. Stanford and M.R. Barnett: *Mater. Sci. Eng. A*, 2009, vol. 516, pp. 226–34.
29. J. Jain, W.J. Poole, C.W. Sinclair, and M.A. Gharghouri: *Scripta Mater.*, 2010, vol. 62, pp. 301–04.
30. J.D. Robson, N. Stanford, and M.R. Barnett: *Scripta Mater.*, 2010, vol. 63, pp. 823–26.
31. J.D. Robson, N. Stanford, and M.R. Barnett: *Acta Mater.*, 2011, vol. 59, pp. 1945–56.
32. J. Geng, Y.B. Chun, N. Stanford, C.H.J. Davies, J.F. Nie, and M.R. Barnett: *Mater. Sci. Eng. A*, 2011, vol. 528, pp. 3659–65.
33. N. Stanford, J. Geng, Y.B. Chun, C.H.J. Davies, J.F. Nie, and M.R. Barnett: *Acta Mater.*, 2012, vol. 60, pp. 218–28.
34. J.F. Nie: *Metall. Mater. Trans. A*, 2012, vol. 43A, pp. 3891–3939.
35. N. Stanford, A.S. Taylor, P. Cizek, F. Siska, M. Ramajayam, and M.R. Barnett: *Scripta Mater.*, 2012, vol. 67, pp. 704–07.
36. J.D. Robson, N. Stanford, and M.R. Barnett: *Metall. Mater. Trans. A*, 2013, vol. 44A, pp. 2984–95.
37. S.R. Agnew, R.P. Mulay, F.J. Polesak, III, C.A. Calhoun, J.J. Bhattacharyya, and B. Clausen: *Acta Mater.*, 2013, vol. 61, pp. 3769–80.
38. J. Jain, P. Cizek, W.J. Poole, and M.R. Barnett: *Acta Mater.*, 2013, vol. 61, pp. 4091–4102.
39. J. Wang and N. Stanford: *Acta Mater.*, 2015, vol. 100, pp. 53–63.
40. J. Jain, P. Cizek, W.J. Poole, and M.R. Barnett: *Mater. Sci. Eng. A*, 2015, vol. 647, pp. 66–73.
41. S.R. Kada, P.A. Lynch, J.A. Kimpton, and M.R. Barnett: *Acta Mater.*, 2016, vol. 119, pp. 145–56.
42. F. Wang, J.J. Bhattacharyya, and S.R. Agnew: *Mater. Sci. Eng. A*, 2016, vol. 666, pp. 114–22.
43. P. Hidalgo-Manrique, J.D. Robson, and M.T. Pérez-Prado: *Acta Mater.*, 2017, vol. 124, pp. 456–67.
44. A. Akhtar and E. Teghtsoonian: *Acta Metall.*, 1969, vol. 17, pp. 1351–56.
45. J.B. Clark: *Acta Metall.*, 1968, vol. 16, pp. 141–52.
46. M.A. Gharghouri, G.C. Weatherly, and J.D. Embury: *Philos. Mag.*, 1998, vol. 78, pp. 1137–49.
47. J.B. Clark: *Acta Metall.*, 1965, vol. 13, pp. 1281–89.
48. M.R. Barnett: *Magnesium Technology 2017*, 1st ed., Springer, Cham, Switzerland, 2017, pp. 143–45.
49. S. Celotto: *Acta Mater.*, 2000, vol. 48, pp. 1775–87.
50. C.H. Caceres and D.M. Rovera: *J. Light Met.*, 2001, vol. 1, pp. 151–56.
51. C.R. Hutchinson, J.F. Nie, and S. Gorsse: *Metall. Mater. Trans. A*, 2005, vol. 36A, pp. 2093–105.

52. P. Hidalgo-Manrique, S.B. Yi, J. Bohlen, D. Letzig, and M.T. Pérez-Prado: *Metall. Mater. Trans. A*, 2013, vol. 44A, pp. 4819–29.
53. F. Siska, L. Stratil, J. Cizek, A. Ghaderi, and M. Barnett: *Acta Mater.*, 2017, vol. 124, pp. 9–16.
54. A. Luque, M. Ghazisaeidi, and W.A. Curtin: *Acta Mater.*, 2014, vol. 81, pp. 442–56.
55. R.L. Fullman and T. Metall: *Soc. AIME*, 1953, vol. 197, pp. 447–50.
56. J.D. Robson: *Acta Mater.*, 2016, vol. 121, pp. 277–87.